



Sacrificial Polymer Substrates in Photopolymerization-Based Micro 3D Printing for Fabrication and Release of Complex Micro Components

Vaut, Lukas; Zeng, Guanghong; Tosello, Guido; Boisen, Anja

Published in:
Advanced Materials Technology

Link to article, DOI:
[10.1002/admt.201900378](https://doi.org/10.1002/admt.201900378)

Publication date:
2019

Document Version
Peer reviewed version

[Link back to DTU Orbit](#)

Citation (APA):
Vaut, L., Zeng, G., Tosello, G., & Boisen, A. (2019). Sacrificial Polymer Substrates in Photopolymerization-Based Micro 3D Printing for Fabrication and Release of Complex Micro Components. *Advanced Materials Technology*, 4(9), Article 1900378. <https://doi.org/10.1002/admt.201900378>

General rights

Copyright and moral rights for the publications made accessible in the public portal are retained by the authors and/or other copyright owners and it is a condition of accessing publications that users recognise and abide by the legal requirements associated with these rights.

- Users may download and print one copy of any publication from the public portal for the purpose of private study or research.
- You may not further distribute the material or use it for any profit-making activity or commercial gain
- You may freely distribute the URL identifying the publication in the public portal

If you believe that this document breaches copyright please contact us providing details, and we will remove access to the work immediately and investigate your claim.

1
2
3
4
5
6
7
8
9
10
11
12
13
14
15
16
17
18
19
20
21
22
23
24
25
26
27
28
29
30
31
32
33
34
35
36
37

Article type: Full Paper

Sacrificial Polymer Substrates in Photopolymerization-based Micro 3D Printing for Fabrication and Release of Complex Micro Components

*Lukas Vaut*¹, Guanghong Zeng, Guido Tosello and Anja Boisen*²*

L. Vaut, Prof. A. Boisen
The Danish National Research Foundation and Villum Foundation's Center for Intelligent Drug Delivery and Sensing Using Microcontainers and Nanomechanics (IDUN), Department of Health Technology, Technical University of Denmark, Kgs. Lyngby, 2800, Denmark
E-mail: ¹ lukv@dtu.dk, ² aboi@dtu.dk

Dr. G. Zeng, DFM A/S (Danish Fundamental Metrology), Hørsholm, 2970, Denmark

Prof. G. Tosello, Department of Mechanical Engineering, Technical University of Denmark, Kgs. Lyngby, 2800, Denmark

Keywords: micro additive manufacturing, sacrificial release layers, 3D microfabrication, micro stereolithography, micro medical device manufacturing

Abstract Text

3D printing technology is widely employed in various scientific disciplines as well as industrial applications such as hearing aid manufacturing. While technological advances and increasing resolution are making 3D printing accessible for microfabrication purposes, one question remains: how can small and delicate components like micro gears, lattices or micro medical devices be released from the build surface of the 3D printer without manual intervention? Herein, a method for 3D printing on top of water-soluble sacrificial substrates made from polyvinyl alcohol (PVA) is presented. Pre-fabricated sacrificial PVA substrates can be mounted onto a customized holder and serve as build surface during the 3D printing operation. The substrates do not only facilitate a mild release of 3D printed objects after dissolution of the sacrificial material, they also potentially allow for a convenient manipulation and further array-based processing of pre-determined patterns of printed structures subsequent to the 3D printing procedure. This, in turn, may enable a full integration into automated production lines. The fabrication of PVA substrates is thoroughly

38 characterized and the 3D printing of various exemplary structures on sacrificial substrates is
39 demonstrated. Finally, the release of 3D printed objects from PVA substrates is shown.

40 **1. Introduction**

41 3D printing has attracted interest since the release of the core inventions of stereolithography
42 (SL) in 1986 and fused deposition modeling (FDM) in 1992, and continues to be a hot
43 topic.^[1,2] The use of 3D printing spans a broad range of applications in different areas such as
44 architecture, automotive industry and medicine. It is used to rapidly produce prototypes as
45 well as functional end-products. Especially in the medical field, 3D printing holds great
46 potential due to the possibility to fabricate customized components with high complexity.
47 Examples of already successful implementations of 3D printing in industrial fabrication of
48 medical products comprise for example dental appliances and hearing aids.^[3,4] Medical and
49 biomedical applications often require miniaturization of products.^[5] Due to advances in
50 resolution and material availability, 3D printing has become a viable alternative to other
51 microfabrication methods in many areas, including biomedical research.^[6] Research efforts in
52 this area cover a broad variety of 3D printed prototypes, ranging from micro medical
53 components such as bioresorbable vascular stents to microscale 3D scaffolds for tissue
54 engineering, oral modified-release dosage forms as well as to propulsion-capable artificial
55 microfish intended for toxin-neutralization applications.^[7-10]

56 As pointed out by Quinlan et al., 3D printing, as of yet, has a low overall build rate when
57 compared to other manufacturing processes, e.g. injection molding, and is therefore
58 potentially less attractive for serial production. However, the start-up as well as maintenance
59 costs related to conventional manufacturing processes like injection molding and machining
60 can be very high, especially when the design complexity of the product increases.^[11] The low
61 capital costs of 3D printing and its inherent flexibility thus makes it increasingly attractive for
62 small to medium scale serial production in industry, for serial production of products that
63 require mass customization (e.g. hearing aids), as well as for the rapid prototyping required in

64 research and development.^[12] When compared to other lithography- or micromachining-based
65 fabrication techniques, micro 3D printing is advantageous as the other techniques are limited
66 with respect to three-dimensional complexity, ease of operation and production of assemblies
67 with moving parts.^[13] One major drawback of 3D printing, however, is the low resolution
68 compared to e.g. photolithography (minimum feature size of 2-3 μm) and electron beam
69 lithography (down to 5 nm).^[14] It must be noted though, that 3D printing resolution is a
70 subject of development and progress is shown on a frequent basis (e.g. custom built 3D
71 printer by Gong et al. with a resolution of 7.6 μm).^[15] Using common digital light processing
72 (DLP)-based SL as well as conventional SL 3D printing, voxel sizes down to 30 μm can
73 easily be achieved.

74 Current micro 3D printing requires manual removal of the printed objects from the build
75 surface by human intervention. This presents an obstacle towards automation and serial
76 production as any component pattern enabling further computer numerical control (CNC) or
77 other array-based processing is corrupted. Additionally, small prints are easily damaged
78 during the manual print removal process. The release of single structures from a common
79 substrate, such as a silicon wafer, by means of a sacrificial release layer, e.g. a water-soluble
80 release layer, is a common procedure in micromachining and microfabrication.^[16] In FDM 3D
81 printing, Polyvinyl alcohol (PVA) and high impact polystyrene (HIPS) are used as built-in
82 sacrificial support structures.

83 Here, we use a rapidly exchangeable solid sacrificial material substrate as the build surface in
84 vat photopolymerization-based 3D printing. The substrate enables further processing steps in
85 an automated production line, and it allows for a mild release by dissolution of the sacrificial
86 material. The working principle of the presented concept is that the solid sacrificial material
87 substrate can be inserted into a vacuum actuated holder (**Figure 1a**). This assembly can be
88 inserted into a desktop DLP-SL 3D printer, in which the PVA substrate serves as the build
89 surface (Figure 1b). Later, the substrate can be utilized for easy manipulation of the 3D

90 printed structures as well as for further processing steps. The PVA substrate can finally be
91 dissolved in water to release the individual 3D printed structures. Advantages of PVA, in this
92 case, include water solubility, chemical resistance against many solvents and
93 biodegradability.^[17]

94 **2. Results and Discussion**

95 **2.1. Compatibility Study using Raman Spectroscopy**

96 As a prerequisite for the presented concept to work, it is of importance to ensure that the
97 contact between the substrate material and the liquid uncured 3D printing photopolymer does
98 not alter the chemical status of the photopolymer and therefore not interfere with the
99 photocuring reaction during the 3D printing procedure. Raman spectroscopy was performed
100 and the spectra (molecular fingerprints) of untreated photopolymer as control and
101 photopolymer after different durations of exposure to potential PVA contamination (1 h, 3 h,
102 1 d, 5 d) compared (**Figure 2**). No changes could be observed and the PVA did not dissolve in
103 the photopolymer or affect it otherwise. Consequently, we conclude that PVA does not alter
104 the chemical status of the photopolymer, does not interfere with the 3D printing process and
105 thus is a suitable substrate material. Supplementary experiments with further 3D printing
106 photopolymers and PVAs support these findings and their results can be found in the
107 supporting information (Figure S 1, Supporting Information).

108 **2.2. PVA Substrate Fabrication**

109 The substrates used in this work for vat photopolymerization 3D printing were fabricated by
110 FDM 3D printing of a precursor substrate and subsequent compression molding (**Figure 3a**,
111 b). This fabrication route has been chosen due to accessibility and increased flexibility with
112 respect to the iterative nature of substrate fabrication optimization. Moreover, it demonstrates
113 the successful fabrication at lab scale with most simple and affordable equipment.

114 To demonstrate the possibility for cheap and scalable substrate production we also performed
115 laser cutting of a sheet of PVA (Figure 3c) as well as direct injection molding of PVA-
116 polymer substrates (Figure 3d).

117 **2.3. Geometrical Characterization of PVA Substrates**

118 For 3D printing, the fabricated PVA substrates must be produced with suitable surface
119 characteristics as well as uniform thickness. It is required that the substrates have sufficient
120 surface flatness to ensure good contact between the substrate and the polymerization interface
121 during the printing procedure, especially when the first layers of the objects are created. The
122 peak-to-valley flatness parameter (FLTt; ISO 12781) was locally probed in areas of 1.27 x
123 0.96 mm using optical profilometry with digital interferometry (DI) and confocal (CF)
124 observation conditions and analyzed after applying a robust gaussian filter (cut-off: 25 μm ;
125 ISO 16610) to eliminate noise, outliers and short-wave details (**Figure 4a**).^[18,19] Different
126 substrates were analyzed: compression molded (CM), hand-roughened (CM-S) and injection
127 molded (IM) PVA substrates. A commercial anodized aluminum 3D printer build platform
128 (BP), plain aluminum substrates (Al) and a silicon wafer (Si) were included as reference
129 substrates. BP and Al substrates served to compare the fabricated PVA substrates to
130 frequently used 3D printing surfaces, Si exclusively served as a quality reference. The
131 analysis of the flatness measurements (**Figure 5a**) shows that, except for CM and Al samples,
132 which exhibit similar flatness (FLTt \approx 2.4 μm ; DI), samples have significantly different FLTt
133 values with large effect sizes (Table S 1, Supporting Information). During the compression
134 molding, the polymer surface adapts the negative of the molds' surface texture. Thus, CM
135 and Al samples have similar flatness as CM substrates were molded with the use of flat
136 aluminum sheets. While BP has the lowest flatness (FLTt \approx 12.11 (DI) and 15.55 μm (CF)),
137 Si has the highest flatness with an FLTt value (0.18 μm ; DI) up to two orders of magnitude
138 lower than the ones of the other samples. In comparison with CM samples (FLTt \approx 3.37 μm ;
139 CF), CM-S samples show a reduced flatness (FLTt \approx 5.46 μm ; CF), which can be explained

140 by the hand-roughening treatment as sanding marks can be observed (Figure 4a). IM samples
141 also show lower flatness ($5.78 \mu\text{m}$; DI) when compared to CM. In the case of IM samples, the
142 surface texture is determined by the manufacturing of the molding tool.

143 The roughness of a surface can affect adhesion and has been found to be associated with the
144 bond strength of adhesives. In this regard, Shahid et al. found that the average roughness (Ra)
145 is linearly correlated with average cleavage strength of steel/adhesive/steel cleavage
146 specimens, probably due to an increase in effective surface area and through the formation of
147 “mini scarf joints on adherend surfaces at micro level”.^[20] Likewise, the successful use of
148 surface roughening treatments for increased adhesive bonding of titanium to polymer
149 composites has been thoroughly discussed.^[21] During the 3D printing procedure, it is
150 fundamental that the first layer of cured photopolymer adheres well to the build surface since
151 the 3D printed objects are subject to tensile stress due to continuous movement of the Z-axis
152 and subsequent separation from the polymerization interface. The local surface roughness,
153 more specifically the arithmetical mean height (S_a), was determined using digital
154 interferometry-based optical profilometry (Figure 4b).^[22] The evaluation of conducted S_a
155 measurements (Figure 5b) show significant differences with large effect sizes between the
156 different samples, except for CM-S ($S_a \approx 573 \text{ nm}$) and IM samples ($S_a \approx 623 \text{ nm}$) (Table S 2,
157 Supporting Information). Si has the lowest roughness ($S_a \approx 2 \text{ nm}$), which matches the
158 specifications of the manufacturer, while BP appears to have the roughest surface ($S_a \approx 1.79$
159 μm). When compared to BP, CM has a significantly lower roughness ($S_a \approx 134 \text{ nm}$). The
160 hand-roughening treatment is seen to greatly increase the roughness of CM-S substrates when
161 compared with CM substrates, which can also be seen in the example of the very complex
162 surface in Figure 4b. Even though CM-S and IM have similar S_a values, the surfaces exhibit
163 very different surface morphologies. The S_a value does not give any indications of the surface
164 morphology and therefore we calculated the developed interfacial area ratio (Sdr), which is a
165 measure for surface complexity and also a better indication of adhesive properties (Figure

166 5c).^[23] The analysis of Sdr values shows significant differences between all samples (Table S
167 3, Supporting Information). The results mainly follow the trend that could be observed in Sa
168 measurements, with better differentiated values for CM-S and IM. The Sdr-value for CM-S
169 was two orders of magnitude higher than for CM.

170 Thickness measurements of different PVA substrates were conducted (Figure 5d), and the
171 measurements on deviation from target thickness show that values obtained for the
172 compression molded PVA substrates (CM) lie in a range of $\approx 26 \mu\text{m}$. In the case of hand-
173 roughened compression molded samples (CM-S) and injection molded samples (IM), the
174 measurements lie in a range of $\approx 43 \mu\text{m}$ and $\approx 23 \mu\text{m}$, respectively. To ensure a successful
175 printing without the need for recurring calibrations, the thickness deviation of the substrates
176 should be smaller than the layer thickness of the individually exposed layers during the 3D
177 printing procedure. As the layer height of the 3D printer in this case was $25 \mu\text{m}$, a thickness
178 deviation above $25 \mu\text{m}$ could call for recurring homing calibrations. The lack of precision in
179 thickness repeatability for CM substrates can partially be explained by the deviation in
180 material dispensing during FDM 3D printing of the precursor substrate. Here, an observed
181 weight deviation with a range of 8.66 mg ($N = 10$) can translate into a $16\text{-}17 \mu\text{m}$ thickness
182 deviation when taking the final substrate dimensions into account and assuming a PVA
183 density of $1.19\text{-}1.31 \text{ g cm}^{-3}$.^[24] Furthermore, the manual handling during the molding
184 procedure leaves room for error. It is to be expected that the thickness deviation is higher for
185 CM-S substrates than for CM substrates, since it is likely that the hand-roughening treatment
186 unevenly affected the final thickness of the substrates. We note that the deviation for CM
187 substrates is not much higher than for injection molded substrates. A further optimization of
188 the CM fabrication processes can lead to a much higher precision in thickness repeatability,
189 allowing for users without access to injection molding to fabricate their own high-quality
190 substrates.

191 Since standard deviations were smaller than $\pm 25 \mu\text{m}$ in all cases, the study was continued
192 based on the same CM fabrication process and without recurring homing calibrations.

193 **2.4. 3D Printing on PVA Substrates**

194 Using a commercial DLP-SL 3D printer and a custom vacuum-actuated holder (see Figure 1a),
195 we were able to 3D print various exemplary structures on CM PVA substrates (**Figure 6**). The
196 workflow allowed us to 3D print arrays of defined geometrical objects on top of PVA
197 substrates and to remove the entire substrate from the holder after the finished 3D printing
198 operation. 3D printed example structures include those, e.g. helical micro-gear and micro-
199 truss lattice, which are nearly impossible to fabricate by other conventional manufacturing
200 techniques, such as injection molding or micromachining.

201 Employing a specifically for this purpose designed and 3D printed test object (Figure 6h) and
202 a texture analyzer, we determined the detachment force to study the relationship between
203 surface characteristics of the build surface and bond strength of the 3D print. In this regard,
204 we interpret the detachment force to be proportional to the bond strength as a higher
205 detachment force is caused by a higher bond strength. The footprint of the test object matches
206 the dimensions of areas probed for the flatness characterization. Arrays of the test object were
207 3D printed on BP, Al, CM and CM-S substrates (**Figure 7a, b, c**) and using a customized
208 texture analyzer setup (Figure 7d), detachment force as well as work of adhesion (area under
209 curve of detachment graph) were determined (Figure 7e). The evaluation of the detachment
210 force (Figure 7f) shows statistically significant differences with large effect sizes between all
211 samples (Table S 4, Supporting Information). Hand-roughening of PVA substrates
212 significantly affected the bond strength between the test objects and CM-S substrates, thus
213 revealing a much higher detachment force when compared to CM substrates. Despite having a
214 rougher surface, Al and BP have lower detachment forces while Al has the lowest. An
215 explanation for this might be the influence of other adhesion promoting factors, which could
216 lead to the occurrence of increased polymer-polymer (cured photopolymer-PVA) interactions.

217 An example for those could be electrostatic adhesion between the PVA substrates and the 3D
218 printed objects according to the electrostatic theory of adhesion, hence leading to a higher
219 bond strength.^[25] This possible explanation is consistent with the observation that the
220 detached 3D printed objects kept sticking to other objects, e.g. the custom microgripper after
221 they have been detached from the PVA substrates. The evaluation of the work of adhesion
222 (Figure 7g) follows a similar trend, except for the fact that no significant difference between
223 BP and AI can be found (Table S 5, Supporting Information).

224 The results indicate that the surface of the proposed PVA substrates may be tailored for
225 optimized performance, e.g. through a surface roughening treatment for increased adhesion of
226 the 3D printed structures to the substrate. However, as already noted in the case of potential
227 influence of electrostatic adhesion, there are most probably further parameters, which can
228 positively or negatively influence the adhesive bond (e.g. surface chemistry and interfacial
229 failure). Moreover, the formation of the adhesive bond itself does not represent the only
230 potential influence that is relevant for a successful 3D printing outcome. As mentioned earlier,
231 the adhesion of 3D printed objects to the substrate was considered to be crucial as the freshly
232 printed layers are subject to tensile stresses caused by the vertical motion of the build platform
233 and the repetitive contact to and separation from the polymerization interface. It is to be
234 expected that the same tensile stresses act on the PVA substrate as well and they could
235 potentially lead to deformation or detachment of the entire PVA substrate. Although these
236 issues could not be detected during the experiments, the different forms of mechanical stress
237 and the consequences they might have should be considered with regards to the potential
238 setting and application of the proposed method.

239 **2.5. Release of 3D Printed Objects from PVA Substrates**

240 An array of helical micro-gears (Figure 6e) 3D printed on CM PVA substrates was released
241 from the substrate within 150 min. (**Figure 8a**; Movie S 1, Supporting Information). Scanning
242 electron microscopy of the harvested individual micro-gears shows that the gears are intact

243 and free of substrate material (Figure 8b, c). The dissolution rate of PVA is highly dependent
244 on the type of PVA (degree of polymerization, degree of hydrolysis) and also on the
245 temperature.^[16] Furthermore, the time needed for the dissolution depends on the amount of
246 material to be dissolved. In Figure 8a it is visible that the PVA substrate was inserted into the
247 dissolution medium in a 90-degree orientation. Since, upon contact with water, the PVA
248 started to dissolve and became rather jelly-like, the substrate lost its mechanical rigidity and
249 deformed. The latter can be observed as a progressing trend within the first 90 minutes. At $t =$
250 90 min some individual released micro-gears were visible, whereas the remnants of the
251 substrate transformed into a clot and engulfed all other micro-gears that were still in contact
252 with the PVA. As a consequence, the PVA needed to be fully dissolved in order to release all
253 3D printed micro-gears, which accounts for the 150 min release time.

254 To illustrate that the release time can be reduced, composite CM PVA substrates with a non-
255 dissolving polylactic acid (PLA) core were fabricated. The PLA core was fully encapsulated
256 by the surrounding PVA and reduced the total amount of PVA by 50%. Using this substrate,
257 the same array of micro-gears could be released within 90 min. (Figure S 2, Movie S 2,
258 Supporting Information). In this case, the non-dissolving PLA core helped to largely maintain
259 the mechanical rigidity of the substrate, so that a clot formation was impossible and only the
260 PVA interfacing the 3D printed micro-gears and the PLA core had to dissolve in order to
261 release all micro-gears. It has to be emphasized that the two experiments are only examples of
262 how the release process could look like, as many influential parameters, such as type and
263 properties of the utilized PVA, have not been investigated. Beyond the dissolution properties
264 of the PVA, factors like excitation type (ultrasound, stirring, flow etc.) and substrate porosity
265 might have a positive influence on diffusion and convection of the dissolving PVA and
266 therefore on the dissolution time. A further optimization of the release procedure can be
267 expected to drastically reduce the required dissolution time.

268

269 **3. Conclusion**

270 In summary, we have demonstrated the use of water-soluble PVA sacrificial substrates in vat
271 photopolymerization-based 3D printing. The fabrication of substrates with suitable flatness,
272 roughness and thickness characteristics was accomplished at lab scale, and their specifications
273 are compatible with industrial fabrication. The substrates were chemically compatible with
274 different 3D printing photopolymers and exhibited good bond strengths to the 3D printed
275 objects. Using a custom-made vacuum-actuated holder, PVA substrates could be rapidly
276 exchanged and taken from the 3D printer, thereby enabling further array-based processing and
277 potential integration into automated production lines. We showed that advanced 3D printed
278 objects can be released through dissolution of the substrate, thereby eliminating the need for
279 manual intervention. Consequently, the proposed method might be potent of promoting the
280 application of 3D printing for the serial production of complex micro components.

281 **4. Experimental Section**

282 *Materials:* All chemicals and reagents were used as received. For the fabrication of PVA
283 substrates different kinds of PVA material were used: RS Pro PVA 3D printing filament (RS
284 Components A/S, Denmark), MOWIFLEX™ C17 and MOWIFLEX™ C600 (Kuraray Nordic
285 Ab Oy, Finland). HTM 140M V2 3D printing photopolymer (EnvisionTEC GmbH, Germany)
286 was used to 3D print onto PVA substrates. Further photopolymers were used for a
287 compatibility study: PIC100 (EnvisionTEC GmbH, Germany) and Form Clear resin
288 (Formlabs GmbH, Germany). 2-propanol (Sigma-Aldrich Denmark A/S, Denmark) was used
289 for the post-treatment of 3D printed structures.

290 *Compatibility study using Raman spectroscopy:* A compatibility assay was performed by
291 incubating 200 mg of solid polyvinyl alcohol (PVA) material in 1 ml of liquid 3D printing
292 photopolymer and analyzing a sample of the liquid after successive timepoints (1 h, 3 h, 1 d, 5
293 d) by Raman spectroscopy. When considering the use of one PVA substrate with a weight of
294 805 mg in the supplied vat of the 3D printer, which is filled with 150 ml of 3D printing

295 polymer, the concentration amounts to 5.37 mg ml⁻¹. The ratio of PVA to 3D printing polymer
296 in the compatibility study was chosen to be multiple times higher. 3D printing polymer which
297 was not in contact with PVA served as control. Raman spectroscopy was employed to
298 determine molecular fingerprints of the samples.

299 Raman spectra were acquired with an in-house-built Raman spectroscopy system with
300 improved sensitivity for Raman scattering registration in case of liquid samples. The system is
301 based on a high power (500 mW) multimode laser with a wavelength of 785 nm. The laser
302 had an intensity of 20 mW μm⁻² and was focused on the sample through a liquid container
303 with a CaF₂ bottom plate. Measurements were carried out with a spectral resolution of 1.8 cm⁻¹
304 in the range from 350 to 2100 cm⁻¹ and collected using a CCD sensor. Wavelength and
305 spectral sensitivity calibration of the instrument was performed according to ASTM 1840 and
306 ASTM E2911 international guidelines.

307 *Fabrication of PVA substrates:* Whereas the FDM-3D printing step did not serve to produce
308 the final substrate, but rather as a material dispensing step to fabricate a precursor substrate of
309 a certain size, the compression molding process acted to transform the precursor into a flat
310 substrate of desired shape by using a mold assembly. For the fabrication of the substrate
311 precursor, a commercially available Original Prusa i3 MK2S desktop 3D printer was used
312 (Prusa Research, Czech Republic) to print with likewise commercially acquired RS Pro PVA
313 filament with a 100% infill, a hotend temperature of 210 °C and a print bed temperature of
314 85 °C (first layer) and 60 °C (following layers). The volume of the substrate precursor was
315 calculated to equal the volume of the mold cavity which is used in the compression molding
316 step. While the FDM 3D printing method can be quite accurate, it is – due to the nature of this
317 technology – not precise enough to exactly dispense the correct volume of material as the
318 layer-by-layer and line-by-line fabrication leads to the creation of small gaps within the print
319 even though the infill ratio is set to 100%. In order to compensate for this phenomenon, the
320 volume of the substrate precursor was increased by 3%, which was found to be an acceptable

321 value to obtain a good substrate after compression molding. After FDM 3D printing of the
322 precursor substrates, the substrates had an average weight of 804.96 mg (N = 10), ranging
323 from 800.09 to 808.75 mg with a standard deviation of 2.93 mg.

324 The mold assembly for the compression molding consisted of a 1 mm thick aluminum mold,
325 90 μ m aluminum foil and 1 mm stainless steel sheets. The compression molding procedure
326 was carried out with a pressure of 55 kN and a temperature of 160 °C using a PW-H HKP300
327 laboratory press (Paul-Otto Weber GmbH, Germany).

328 For some of the resulting substrates, the surface was modified by sanding one side with 600
329 grit sanding paper.

330 Composite compression molded substrates consisting of PVA and polylactic acid (PLA) were
331 as well fabricated using an FDM 3D printing and a compression molding step. PLA inserts
332 were 3D printed with smaller dimensions, constituting 50 % of the final substrate. PVA
333 substrates were designed to have a cavity and the 3D printing procedure was paused as soon
334 as the cavity was completed. Then the PLA insert was inserted into the cavity and the 3D
335 printing procedure was continued. The cavity was closed with the remaining layers of PVA,
336 thereby fully engulfing the PLA in its' core. The compression molding step transformed the
337 precursor composite substrates into smooth PLA-PVA core-shell substrates of 1 mm thickness
338 using the same conditions as with plain PVA substrates.

339 In a different approach, a Press 300 SV laboratory platen press (Dr. Collin GmbH, Germany)
340 served to transform 15 g of MOWIFLEXTM C17 PVA polymer pellets into a compressed
341 sheet using a pressure of 50 bar and a temperature of 150 °C for a duration of 1000 s and
342 subsequently cooling it down to 30 °C within 500 s. Substrates of desired shape were cut from
343 the sheet with an Epilog Mini 18 laser cutter (Epilog Laser BV, The Netherlands) which was
344 equipped with a 30 W CO₂ laser. This procedure needed to be performed with the necessary
345 safety precautions as toxic fumes can be release during the procedure.^[24]

346 Injection molding of PVA substrates was performed using an Arburg Allrounder 370A
347 injection molding machine (Arburg GmbH & Co KG, Germany) equipped with an 18mm
348 screw and MOWIFLEX™ C600 PVA polymer. Injection molding parameters were adjusted
349 to 70 bar back pressure, 180 °C melt temperature, 40 °C mold temperature, 50 mm s⁻¹
350 injection velocity, 500 bar packing pressure, 10 s packing time and 40 s cooling time.

351 *Characterization of PVA and reference substrates:* The thickness of the fabricated substrates
352 was measured in the center and in the four corners of each substrate using an RS Pro
353 micrometer screw with an error of 0.001 mm (RS Components, Denmark). A PLu neox
354 optical 3D profiler (Sensofar Metrology, Spain) served to conduct surface topology
355 measurements, using confocal and interferometric microscopy. To analyze the flatness
356 property of the various specimen, 10X interferometry and 20X confocal lenses were used for
357 data acquisition. To compensate the loss in field of view when using the 20X confocal lens,
358 stitching was used to combine four images to one bigger area image. A 50X interferometry
359 lens was used to acquire data for the analysis of the surface roughness. In case of all
360 specimens, a sampling procedure based on a 20 x 20 mm grid was performed to obtain surface
361 measurements in a total of 25 spots in always the same relative positions. A 3” silicon wafer
362 (No. 16013, Ted Pella inc., USA) with a specified roughness and total thickness variation of 2
363 nm and <20 μm, respectively, as well as the supplied build platform of an EnvisionTec Micro
364 Plus High-Res DLP 3D printer were used as reference surfaces. Treatment and analysis of
365 surface metrology data was done in SPIP 6.7.4 (Image Metrology A/S, Denmark) analytical
366 software.

367 *Computer aided design (CAD):* All design tasks were carried out using SolidWorks 2015
368 (Dassault Systèmes SolidWorks Corporation, USA) and OpenSCAD open source software.

369 *Machining of customized 3D printer build platform:* A customized 3D printing build platform
370 featuring a four-point spring leveling mechanism and a vacuum-actuated holding cavity for a
371 print substrate was made to retrofit a Micro Plus High-Res digital light processing (DLP) 3D

372 printer (EnvisionTec GmbH, Germany). The platform was machined by an external
373 machining shop using a combination of CNC milling and electrical discharge machining.

374 *3D printing on PVA substrates:* The 3D printing on PVA substrates was conducted with an
375 EnvisionTec Micro Plus High-Res DLP 3D printer with a XY resolution of 30 μm pixel size
376 and a Z resolution of 25 μm . The 3D printer was retrofitted with a customized build platform
377 to enable a flush leveling of the platform to the polymerization interface of the printer.

378 Perfactory RP software (EnvisionTEC GmbH, Germany) served to create print files from the
379 prepared CAD models. After the printing procedure, the PVA substrate with printed structures
380 on top was first cleaned from excess printing material in a beaker with 2-propanol placed in
381 an ultrasound bath for 5 min and subsequently post-cured in an UV oven for 10 min
382 (EnvisionTEC GmbH, Germany).

383 *Scanning electron microscopy:* All scanning electron microscopy was performed using a
384 TM3030Plus tabletop scanning electron microscope (Hitachi High Technologies Europe
385 GmbH, Germany). A 208HR high resolution sputter coater (Cressington Scientific
386 Instruments, UK) equipped with a gold target was used to coat the specimens with a thin layer
387 of gold (≈ 20 nm) prior to observation.

388 *Determination of detachment force:* A TA.XT plus Texture Analyzer (Stable Micro Systems,
389 UK) equipped with a 10 kg load cell and a customized probe was used to measure detachment
390 forces needed to separate a printed sample from different 3D printing substrates. Detachment
391 forces and work of adhesion were computed with a customized python program.

392 *Release of micro 3D prints from PVA substrates:* 3D printed structures were released from the
393 PVA substrate by retaining the substrate in a small box with a bottom of fine stainless-steel
394 mesh and placing it in a de-ionized water-filled beaker, which in turn was placed into an
395 ultrasound bath at a temperature of 55 $^{\circ}\text{C}$. The samples were kept in the ultrasound bath until
396 all PVA was dissolved. A waterproof USB endoscopic camera and Video Velocity Free
397 software (Candy Labs Media, Canada) were used to record time-lapse photos during the

398 release procedure. The samples were ultimately taken out of the water and left to dry in an
399 oven at 37 °C.

400 *Statistics:* All presented statistics were computed using R programming language and RStudio
401 software (RStudio Inc., USA) as well as Microsoft Excel (Microsoft Corporation, USA). As
402 in case of reference samples Si and BP only one specimen was available each, t-test results
403 comparing those with Alu, CM, CM-S and IM samples are based on the assumption that the
404 measured reference samples constitute ideal and representative samples of their kind. The
405 results obtained in these cases can serve as an indication only, because resulting p-values
406 might be distorted. Consequently, the reported effect sizes (Hedges' g) are more reliable.

407 **Supporting Information**

408 Supporting Information is available from the Wiley Online Library or from the author.

409

410 **Acknowledgements**

411 The authors would like to acknowledge the Center for Intelligent Drug Delivery and Sensing
412 Using Microcontainers and Nanomechanics (IDUN) whose research is funded by the Danish
413 National Research Foundation (DNRF122) and Villum Fonden (Grant No. 9301).

414

415 Dr. Guanghong Zeng acknowledges funds from the Danish Agency for Institutions and
416 Educational Grants, metrology for additively manufactured medical implants (short name:
417 MetAMMI, project number: 15HLT09) from the EMPIR program. The EMPIR program is
418 co-financed by the participating states and the European Union's Horizon 2020 research and
419 innovation program.

420

421 The authors would also like to thank Dr. Kristian E. Jensen and Dr. Tommy Sonne Alstrøm
422 for help with the manuscript preparation, Francesco Regi for performing injection molding
423 and Jesper Scheel for photography. Furthermore, the authors would like to thank Ann-Britt
424 Aspholm-van der Brugge and Kuraray Nordic Ab Oy for straightforward communication,
425 great service and provision of free polymer samples.

426

427 **Conflict of Interest**

428 The authors declare no conflict of interest.

429

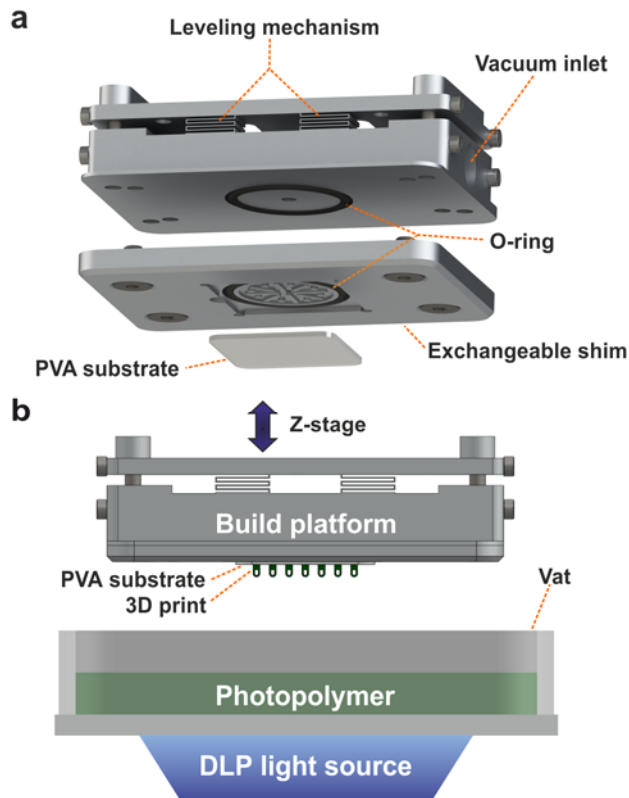
430

431

432 References

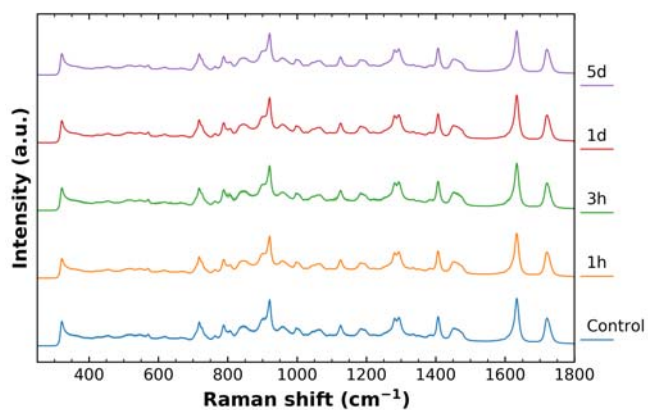
- 433 [1] C. W. Hull (UVP Inc.), *US 4575330* **1986**.
- 434 [2] S. S. Crump (Stratasys Inc.), *US 5121329* **1992**.
- 435 [3] N. Hopkinson, R. J. M. Hague, P. M. Dickens, *An Industrial Revolution for the Digital*
436 *Age*, Wiley, Hoboken, NJ, USA, **2006**.
- 437 [4] C. G. Sandström, *Technol. Forecast. Soc. Change* **2016**, *102*, 160.
- 438 [5] L. Alting, F. Kimura, H. N. Hansen, G. Bissacco, *CIRP Ann.* **2003**, *52*, 635.
- 439 [6] B. Gross, S. Y. Lockwood, D. M. Spence, *Anal. Chem.* **2017**, *89*, 57.
- 440 [7] R. van Lith, E. Baker, H. Ware, J. Yang, A. C. Farsheed, C. Sun, G. Ameer, *Adv. Mater.*
441 *Technol.* **2016**, *1*, 1.
- 442 [8] N. A. Chartrain, C. B. Williams, A. R. Whittington, *Acta Biomater.* **2018**, *74*, 90.
- 443 [9] J. Wang, A. Goyanes, S. Gaisford, A. W. Basit, *Int. J. Pharm.* **2016**, *503*, 207.
- 444 [10] W. Zhu, J. Li, Y. J. Leong, I. Rozen, X. Qu, R. Dong, Z. Wu, W. Gao, P. H. Chung, J.
445 Wang, S. Chen, *Adv. Mater.* **2015**, *27*, 4411.
- 446 [11] H. E. Quinlan, T. Hasan, J. Jaddou, A. J. Hart, *J. Ind. Ecol.* **2017**, *21*, S15.
- 447 [12] C. Kapetaniou, A. Rieple, A. Pilkington, T. Frandsen, P. Pisano, *Technol. Forecast.*
448 *Soc. Change* **2018**, *128*, 22.
- 449 [13] M. Vaezi, H. Seitz, S. Yang, *Int. J. Adv. Manuf. Technol.* **2013**, *67*, 1721.
- 450 [14] A. Pimpin, W. Srituravanich, *Eng. J.* **2012**, *16*, 37.
- 451 [15] H. Gong, B. P. Bickham, A. T. Woolley, G. P. Nordin, *Lab Chip* **2017**, *17*, 2899.
- 452 [16] V. Linder, B. D. Gates, D. Ryan, B. A. Parviz, G. M. Whitesides, *Small* **2005**, *1*, 730.
- 453 [17] C. A. Finch, *Polyvinyl Alcohol, Properties and Uses*, Wiley, Hoboken, NJ, USA, **1973**.
- 454 [18] *ISO 12781-1:2011 - Geometrical Product Specifications (GPS) -- Flatness -- Part 1:*
455 *Vocabulary and Parameters of Flatness*, International Organization For
456 Standardization, Vernier, Geneva, Switzerland, **2011**.
- 457 [19] *ISO 16610-71:2014 - Geometrical Product Specifications (GPS) -- Filtration -- Part*

- 458 71: *Robust Areal Filters: Gaussian Regression Filters*, International Organization For
459 Standardization, Vernier, Geneva, Switzerland, **2014**.
- 460 [20] M. Shahid, S. A. Hashim, *Int. J. Adhes. Adhes.* **2002**, *22*, 235.
- 461 [21] P. Molitor, V. Barron, T. Young, *Int. J. Adhes. Adhes.* **2001**, *21*, 129.
- 462 [22] *ISO 25178-2:2012 - Geometrical Product Specifications (GPS) -- Surface Texture:*
463 *Areal -- Part 2: Terms, Definitions and Surface Texture Parameters*, International
464 Organization For Standardization, Vernier, Geneva, Switzerland, **2012**.
- 465 [23] R. Leach, *Characterisation of Areal Surface Texture*, Springer Berlin Heidelberg,
466 Berlin, Heidelberg, **2013**.
- 467 [24] ILO, WHO, "ICSC 1489 Polyvinyl alcohol,"
468 https://www.ilo.org/dyn/icsc/showcard.display?p_lang=en&p_card_id=1489&p_version=2,
469 accessed: 09, 2018.
- 470 [25] W. C. Wake, *Polymer (Guildf)*. **1978**, *19*, 291.
- 471 [26] L. Rose, "Internal Structures for SLA, DLP, or SLS style printing,"
472 <https://www.thingiverse.com/thing:1394337/files>, accessed: 03, 2018.
- 473
- 474

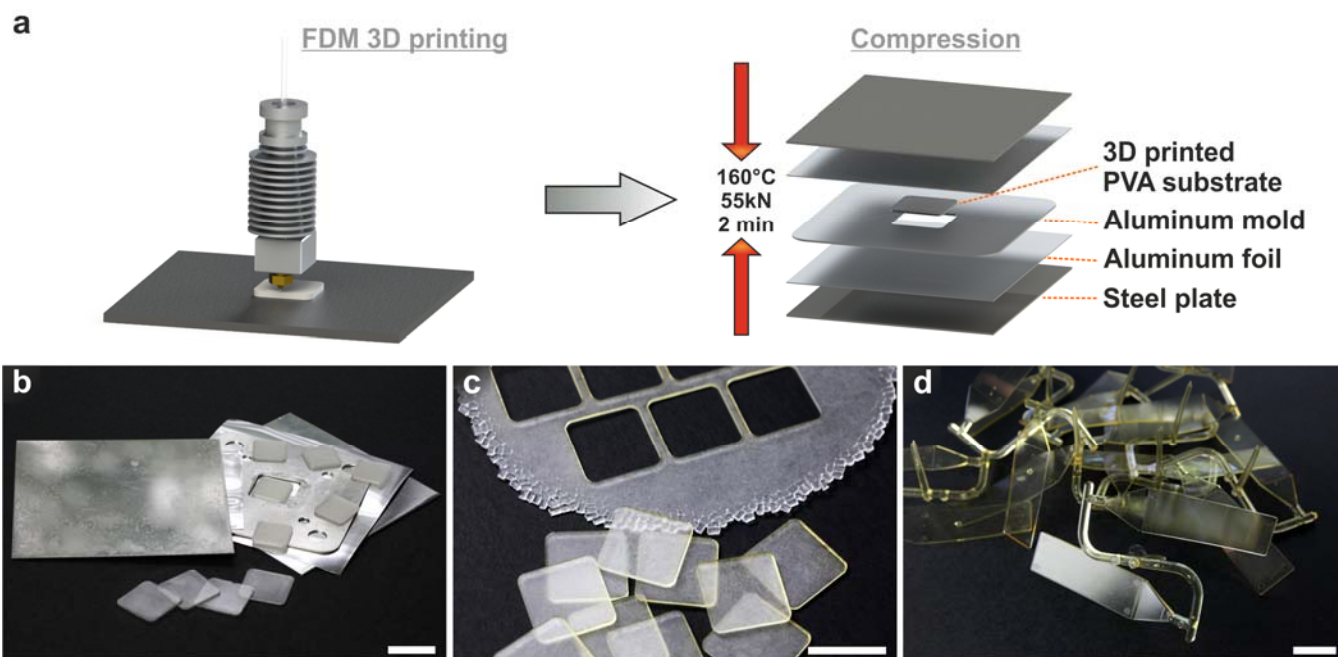


475
 476
 477
 478
 479
 480
 481
 482
 483

Figure 1. a) Design of customized vacuum-actuated substrate holder for the use in a desktop DLP-SL 3D printer. b) Schematic illustration of working principle of using pre-fabricated PVA substrates in a DLP-SL 3D printer. The PVA substrate is used as the build surface and held in place by the vacuum-actuated holder (build platform) which moves in Z direction. In an industrial production line setting, the holder could be operated by a robotic arm which also carries out further processing steps.

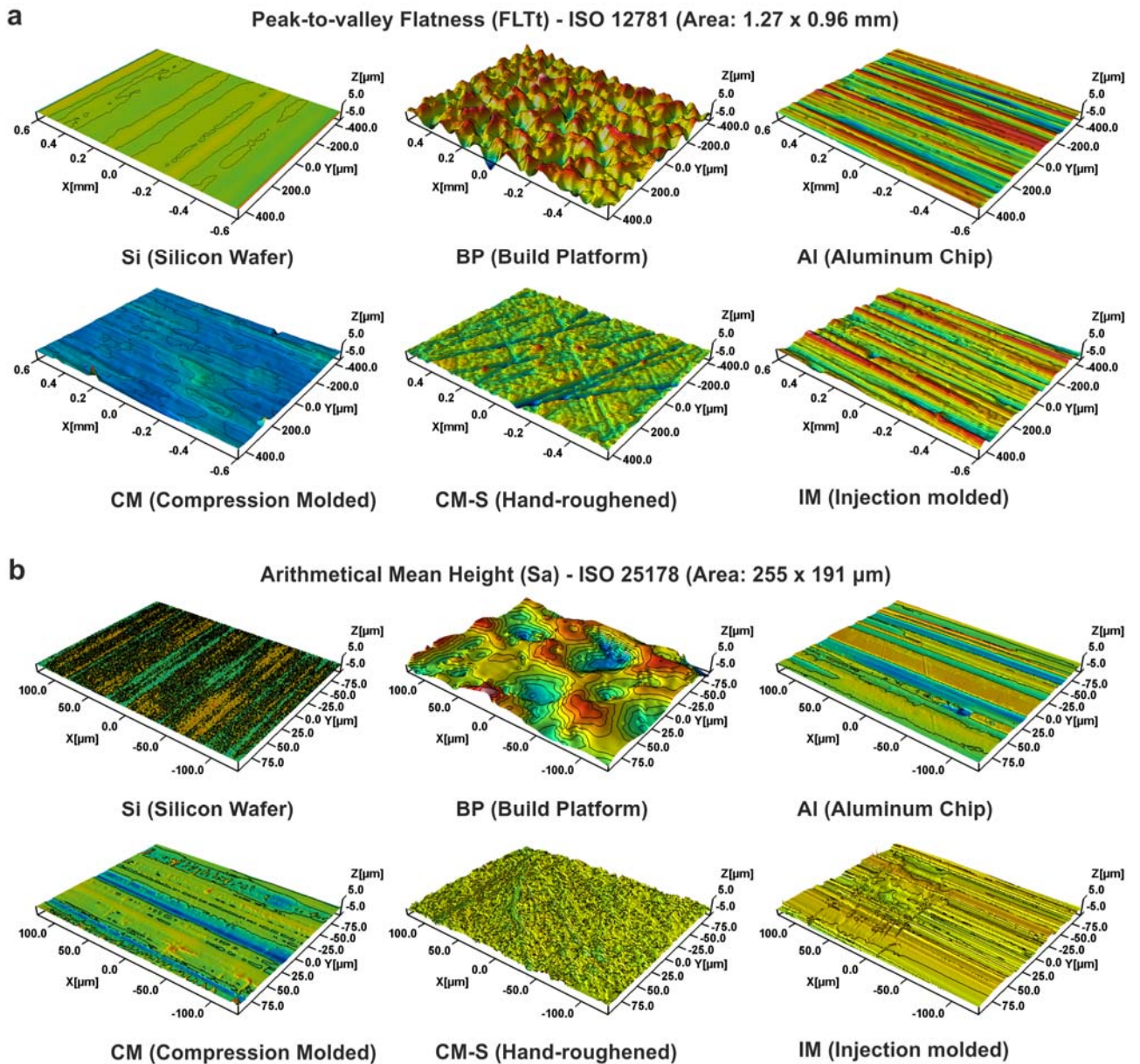


484
485 **Figure 2.** Molecular fingerprint of HTM 140 M 3D printing photopolymer after contact with
486 RS Pro PVA filament for different time durations (1 h, 3 h, 1 d and 5 d) and untreated
487 (Control), as determined by Raman spectroscopy.
488



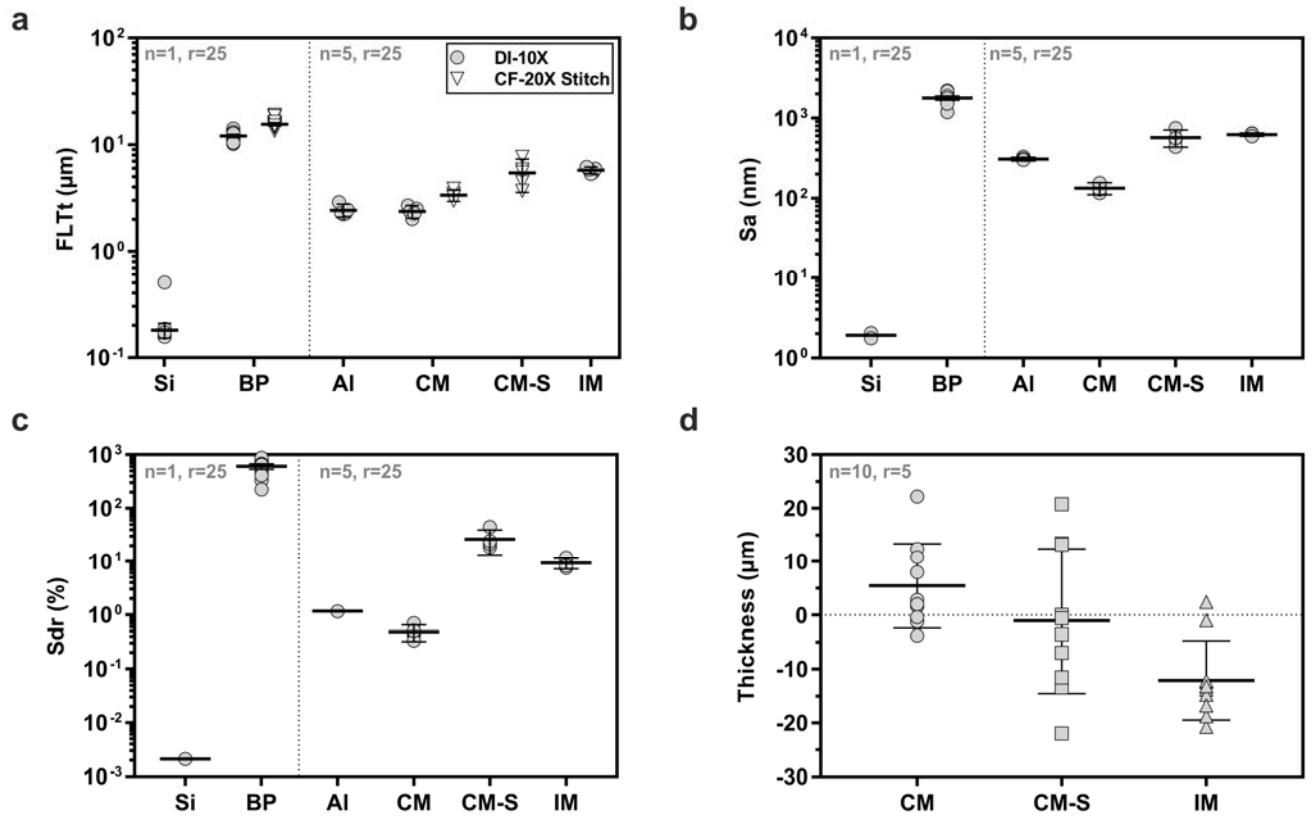
489
 490 **Figure 3.** PVA substrate fabrication. a) Schematic illustration of two-step PVA substrate
 491 fabrication sequence using fused deposition modelling (FDM) 3D printing and subsequent
 492 compression molding. b-d) Photographs of differently fabricated PVA substrates. b) FDM 3D
 493 printed precursor substrates (substrates placed on mold assembly) and compression molded
 494 substrates (front). c) Laser-cut substrates from compressed PVA sheet. d) Injection molded
 495 PVA substrates in standard object slide format. Scale bars are equal to 25 mm.
 496

POST-PRINTED



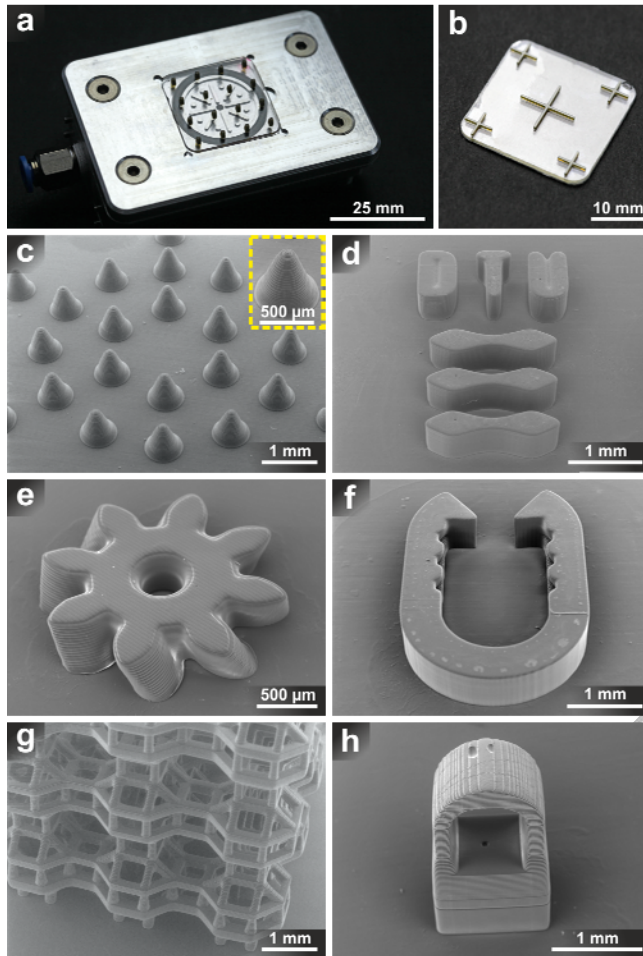
497
498
499
500
502
503
504
505

Figure 4. Flatness and roughness measurements obtained by optical profilometry. a) Representative surface renderings of substrates used for flatness analysis. Computed from data acquired with a 20X confocal lens in stitching mode (BP, CM and CM-S) and a 10X interferometry lens (Si, Al and IM). b) Representative surface renderings of data used for roughness analysis (Sa and Sdr). Computed from acquisitions with a 50X interferometry lens.



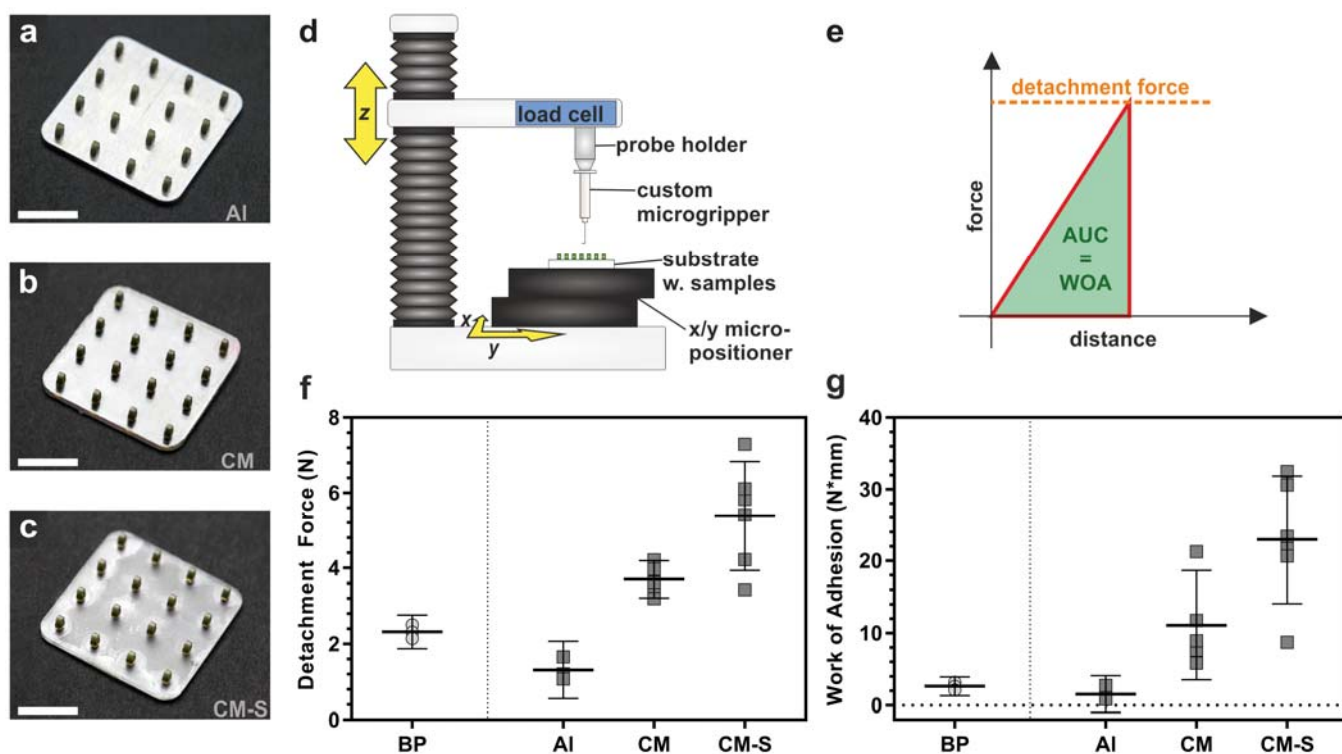
506
 507
 508
 509
 510
 511
 512
 513
 514
 515
 516
 517
 518
 519
 520
 521
 522

Figure 5. Geometrical characterization of different 3D printing substrates: Plain aluminum (Al), compression molded (CM), hand-roughened CM (CM-S) and injection molded (IM) PVA and reference substrates: Silicon wafer (Si) and commercial anodized 3D printer build platform (BP). Error bars represent 95% confidence interval in a), b) and c) and standard deviation in d). a) Peak-to-valley flatness deviation (FLTt) measurements from optical profilometry surface data obtained with digital interferometry (DI) and confocal (CF) observation conditions. For statistical comparison see Table S 1. b) Arithmetical mean height (Sa) measurements from optical profilometry surface data. For statistical comparison see Table S 2. c) Developed interfacial area ratio (Sdr) computed from optical profilometry surface data. Statistical comparison available in Table S 3. For a), b) and c) counts: N=5 with 5 different samples in case of Al, CM, CM-S and IM and N = 1 with 25 repeated measurements on the same sample in case of Si and BP. d) Micrometer thickness measurements of PVA substrates adjusted to target values with $Y = 0 =$ target thickness value. N = 10.



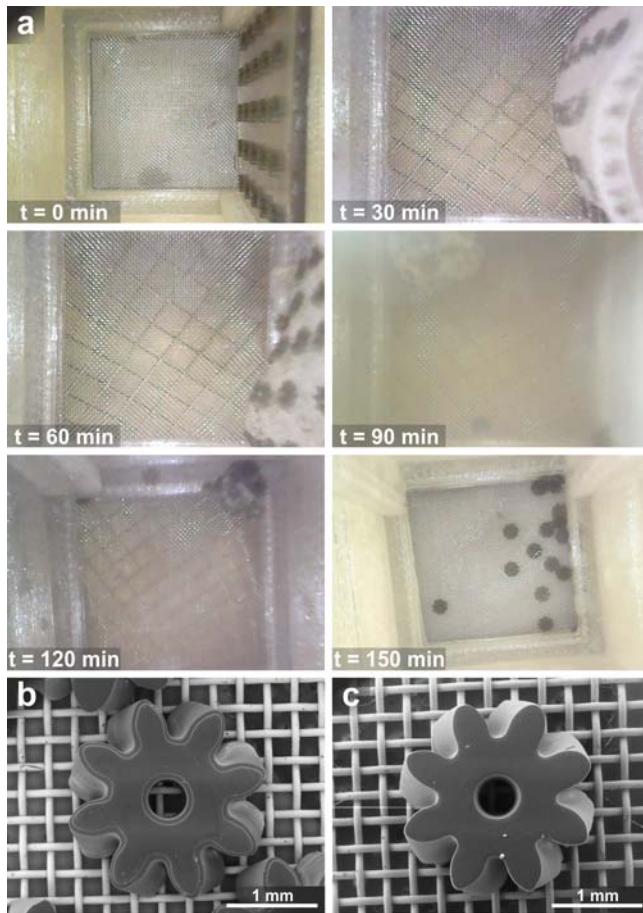
524
 525
 526
 527
 528
 529
 530
 531
 532
 533

Figure 6. Photographs and SEM micrographs of 3D printed structures on compression molded PVA substrates (CM). a) Array of printed structures on PVA substrate inserted in vacuum-actuated holder (see schematics in Figure 1a and b). b) 3D printed crosshairs, facilitating evaluation of alignment of PVA substrate and printed structures. c) Circular array of micro-cones. d) DTU logo assembly from separate 3D printed parts. e) Helical micro-gear with a twist of 25° . f) Surgical staple. g) Complex lattice made from micro-sized trusses.^[26] h) Small structure used for evaluation of bond strength of 3D print to PVA substrate.



534
 535 **Figure 7** Determination of detachment forces/bond strengths of 3D printed objects on PVA
 536 substrates. a-c) Photographs of manufactured samples. Scale bars are equal to 10 mm. a) Test
 537 structures 3D printed on plain aluminum substrates (Al). b) Test structures 3D printed on
 538 compression molded PVA substrates (CM) and c) hand-roughened CM PVA substrates (CM-
 539 S). d) Schematic illustration of texture analyzer test-setup used for the experiments. e)
 540 Schematic illustration of obtained displacement curves. f) Evaluation of detachment forces. g)
 541 Determined work of adhesion (WOA), which is equal to the area under the curve (AUC) of
 542 the displacement graph. Additional to the manufactured samples, a commercial 3D printer
 543 build platform (BP) also served as reference substrate. N = 3-6. Error bars represent 95%
 544 confidence interval. Statistical evaluation available in Table S 4 and Table S 5.

545
 546
 547



548
 549
 550
 551
 552
 553
 554
 555
 556
 557
 558
 559
 560

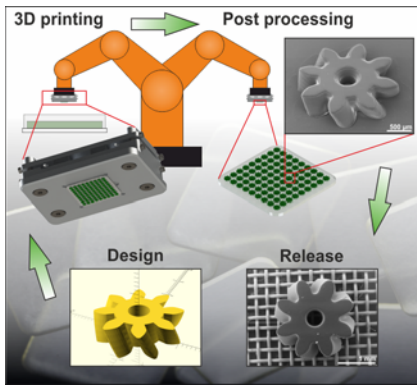
Figure 8. Release of 3D printed objects from PVA substrates. a) Time-lapse photos taken with a water-resistant endoscopic camera during the release procedure of 3D printed micro-gears from compression molded PVA substrates (CM). Release procedure was carried out in a customized release-chamber/substrate-holder combination at 55 °C in an ultrasound bath. b) and c) SEM micrographs of 3D printed helical micro-gears (see Figure 6e) on stainless steel filtering mesh after dissolution of compression molded PVA substrates (CM) and subsequent release. b) front side. c) backside.

561 **3D printing on top of sacrificial substrates** is demonstrated. The used 3D printing workflow
562 enables the 3D printing on quickly exchangeable substrates, further array-based processing of
563 3D printed products and easy manipulation, as well as integration into industrial production
564 lines. 3D printed products can be mildly released from the substrates upon dissolution of
565 sacrificial material and harvested.

566
567 **3D printing**

568
569 **L. Vaut, G. Zeng, G. Tosello, A. Boisen**

570
571 **Sacrificial Polymer Substrates in Photopolymerization-based Micro 3D Printing for**
572 **Fabrication and Release of Complex Micro Components**
573



574
575